

文章编号:1000-0550(2025)03-0961-15

末次盛冰期以来浑善达克沙地光释光年代学及气候变化研究

田娅琪¹,周亚利¹,孙晓巍¹,张岳敏¹,炊郁达²

1.陕西师范大学地理科学与旅游学院,西安 710119

2.中国科学院地球环境研究所,西安 710061

摘要【目的】浑善达克沙地位于内蒙古中东部东亚季风区的尾闾地带,因其独特的地理环境和沙地内广泛发育的风成沉积而成为研究末次盛冰期以来气候变化的理想区域。以往对浑善达克沙地的年代学研究主要集中于全新世,末次盛冰期以来的研究因缺少系统的地层年代框架而相对较少。【方法】以浑善达克沙地南缘蓝旗南(LQS)和八楞山(BLS)两个风沙沉积序列剖面为研究对象,利用光释光(Optical Stimulated Luminescence, OSL)测年方法中的单片再生剂量法(Single-Aliquot Regenerative-dose, SAR)进行地层年代框架的测定,并综合沉积特征、粒度及石英颗粒表面形态特征进行分析。【结果】18.0~11.5 ka,沙地主要发育风成砂与砂黄土互层,气候较为冷干,风沙活动强烈,存在千年尺度气候波动。11.5~8.2 ka,温度波动上升,气候相对干冷,主要发育沙层,8.94 ka 和 8.20 ka 发育的砂质古土壤指示了全新世早期,沙地气候由冷干逐渐转为暖湿。8.2~2.7 ka,气候最为温暖湿润,两剖面均发育砂质古土壤。2.7 ka 至今,气候温和偏干,发育弱砂质古土壤。【结论】整体来看,末次盛冰期以来浑善达克沙地的气候快速变化具有全球性和普遍性特征,与东亚季风紧密相关,受太阳辐射和全球冰量的共同驱动,是对全球气候变化的区域响应。

关键词 浑善达克沙地;光释光测年;末次盛冰期;气候变化

第一作者简介 田娅琪,女,1998年出生,硕士研究生,释光年代学及环境演化,E-mail: 1679385754@qq.com

通信作者 周亚利,女,副教授,E-mail: ylzhou109@163.com

中图分类号 P534.63 **文献标志码** A

DOI: 10.14027/j.issn.1000-0550.2023.053

CSTR: 32268.14/j.cjxb.62-1038.2023.053

0 引言

干旱、半干旱地区约占全球陆地面积的41%,因其降水稀少、土壤贫瘠、生态环境脆弱,对气候变化和人类活动响应极为敏感,成为国际社会关注的热点地区^[1]。浑善达克沙地作为中纬度亚洲内陆干旱区之一,既是东亚季风性气候与大陆性气候的过渡地带,又是我国北方沙漠—黄土边界带和农牧交错带^[2]的重要组成部分。该地区气候变率高,对气候变化具有放大效应,因而成为研究气候变化的理想区域。截至目前,已有众多学者对浑善达克沙地的沙漠化、时空演化及古环境、古气候演变进行了相关研究。巴彦淖尔湖相—风成沉积序列的¹⁴C测年结果及沉积特征的分析结果表明,受东亚夏季风雨带迁

移的影响,全新世早期气候最为湿润,4.2 ka之后开始变干^[3],沙地边缘黄土沉积重建的末次盛冰期以来的降水变化趋势与之类似^[4]。达里湖湖泊沉积物及湖岸线反映的高水位也记录了在早全新世降水已达最大值^[5-6]。泊江海子地区沉积物岩心以¹⁴C测年为框架重建的末次冰消期以来的气候变化特征也支持全新世早期气候最为湿润的观点^[7]。与之不同的是,达里湖沉积物有机质的碳氮特征表明,全新世早期湖泊的水位和生产力逐渐增加,全新世中期湖泊水位进一步上升,碳氮浓度稳定在最高值^[8]。同时,也有大量风成沉积记录显示,浑善达克沙地在全新世中期降水量达到最大^[9-11]。李森等^[12]等根据粒度、化学元素和孢粉等指标特征分析,将全新世划分为升温波动期、温暖期和温干冷干波动期。沙地东北—西

收稿日期:2023-04-17;修回日期:2023-06-15;录用日期:2023-07-17;网络出版日期:2023-07-17

基金项目:国家自然科学基金项目(42071112)[Foundation: National Natural Science Foundation of China, No. 42071112]

南断面上10个沙丘的光释光测年结果表明,在全新世中期沙丘总体上处于固定半固定状态^[13]。以上研究表明,浑善达克沙地不同地理位置不同地质载体或相同地质载体不同气候指标反映的末次盛冰期以来的气候变化存在较大差异,这种差异是由于测年手段不同引起的还是由于不同气候指标反映的气候差异引起的还有待进一步研究。

在沙漠/沙地广布的干旱半干旱地区,风成/湖泊沉积及其地层序列是气候环境演化独特而重要的地质档案^[14-15]。但是,由于沙漠/沙地地表侵蚀和堆积速率较快,记录较长时间尺度气候变化的地层剖面往往不易寻找,并且缺乏系统可靠的年代数据和合适的测年方法^[16-17]。以往对浑善达克沙地的研究主要集中于全新世,缺乏更长时间尺度的气候环境变化研究。近年来,光释光(OSL)测年技术被广泛应用于第四纪沙漠/沙地沉积物测年^[18-22]。光释光测年技术较¹⁴C测年和热释光测年方法消除了“碳库效应”及释光信号残留对测年结果的影响,提高了测年准确度,扩展了测年上限,测年范围可达几百年至几十万年^[23]。虽然记录浑善达克沙地气候变化的年龄数据在过去十几年中迅速增加^[24-28],但对末次盛冰期以来的研究还需要加强和深入。

本文利用OSL测年技术对浑善达克沙地南部两个风沙沉积剖面的地层序列进行研究,建立了末次盛冰期以来的地层年代框架,并结合粒度和石英表面形态特征对沙地末次盛冰期以来的气候变化过程进行分析,揭示了沙地气候变化的规律和机制以及

与全球气候事件之间的联系。

1 研究区概况与研究材料

浑善达克沙地位于内蒙古高原东部地区,东起大兴安岭西麓达里诺尔以东的低山丘陵区,南倚燕山丘陵北麓,西抵集二铁路戈壁荒漠区,北至锡林浩特、阿巴嘎旗。东西长约450 km,南北宽约300 km,总面积可达 $2.71 \times 10^4 \text{ km}^2$,地势东南高西北低。沙地地处我国北方干旱一半干旱地区,属于中温带干旱半干旱大陆性季风气候,年平均气温介于0.9 ℃~5.5 ℃,年平均降水量介于240.3~422.6 mm^[2]。地貌以固定一半固定沙丘为主,流动的新月形沙丘和沙丘链为辅,因受西北风的影响,沙丘大致沿西北—东南东方向展布。东部和中部有锡林河、公格尔音郭勒河及高格斯台河,东南部有滦河,中西部则多为汇入湖泊或消失于沙地的内流河^[11,29]。沙地内湖泊十分发育,沿东西向断裂带有若干湖盆分布(图1)。

通过对浑善达克沙地进行详细实地考察,选取沙地南缘蓝旗南(LQS)和八楞山(BLS)两处出露较好的风沙沉积序列作为研究对象。LQS和BLS两个剖面自上而下地层分别为灰黑色砂质古土壤—湖相砂—砂黄土、砂质古土壤—风成砂—砂黄土互层(图2)。根据沉积物的颜色、结构等特征划分不同地层,在每层沉积相顶部和底部用不锈钢管共采集15个光释光样品及其对应的沉积学样品。LQS和BLS剖面沉积序列的具体沉积特征描述见表1。

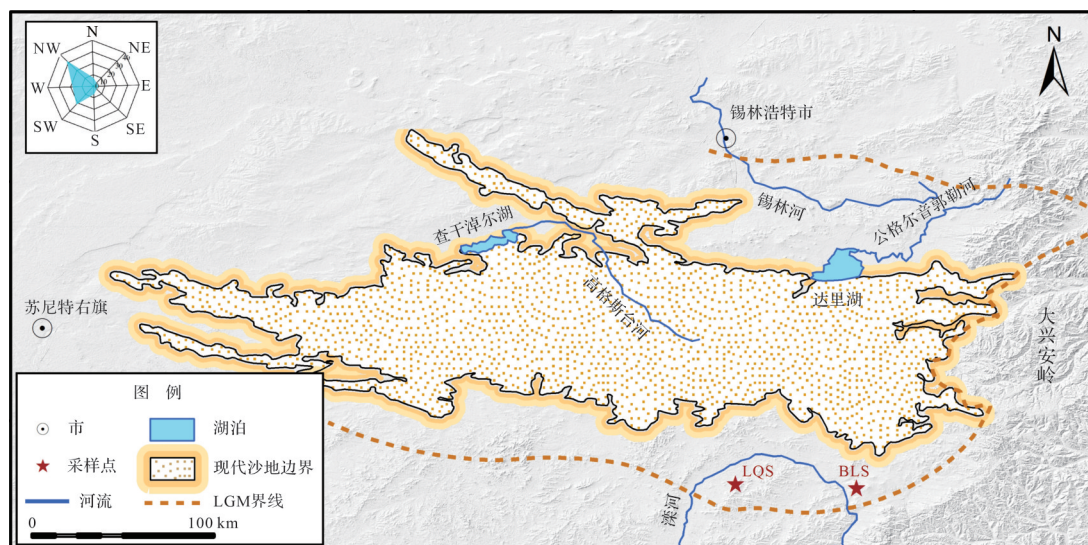


图1 浑善达克沙地区域、采样点位置及末次盛冰期沙地边界^[25]

Fig.1 Location of the study area, sampling sites, and border of the Otindag sandy land during the Last Glacial Maximum^[25]

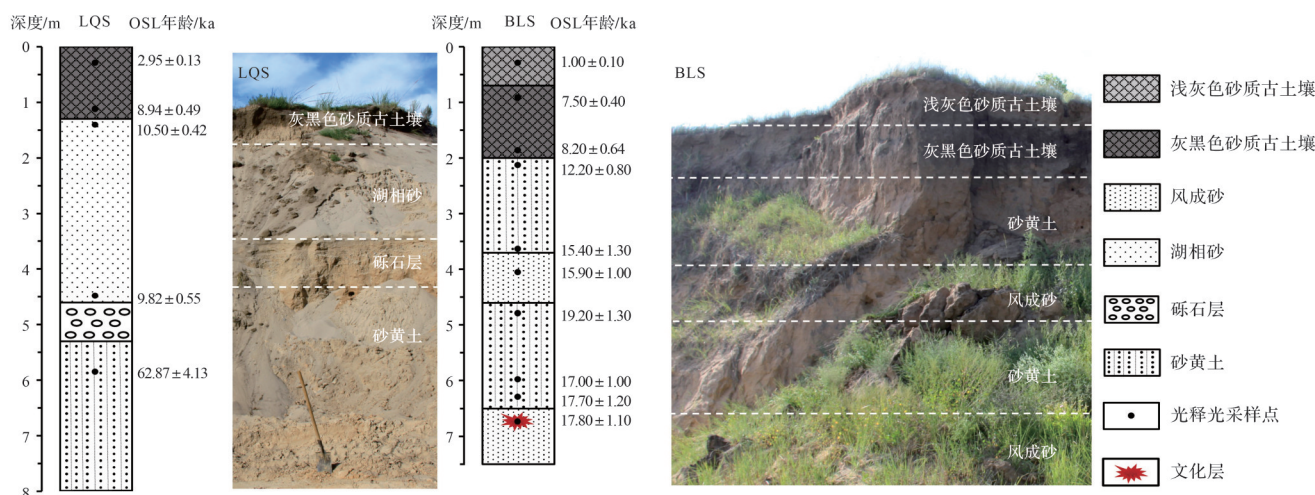


图2 浑善达克沙地LQS、BLS剖面地层序列及各沉积地层照片

Fig.2 Stratigraphic sequence and sedimentary photos of the Lanqi South (LQS) and Baleng Mountain (BLS) profiles in Otindag sandy land

表1 LQS和BLS剖面地层划分和特征描述

Table 1 Division and stratigraphic description of the LQS and BLS profiles

剖面	深度/m	地层沉积学特征描述
LQS	0~1.3	灰黑色砂质古土壤,颜色由上至下逐渐变浅。湿润时为灰黑色,干燥时为棕黄色,粗砂质地,垂直节理发育,含有植物根系
	1.3~4.6	白色湖相砂层,粗砂,质地疏松,发育水平层理
	4.6~5.3	黄色粗砂层,含砾石,水平层理发育
	5.3~8.0以下	浅棕色砂黄土,细砂—中砂,质地较疏松,未见底
BLS	0~0.7	浅灰色砂质古土壤,细砂质地,较松软,有草根,与下部砂质土界限明显,可能有沉积间断
	0.7~2.0	灰黑色砂质古土壤,极细砂,质地较坚硬,发育垂直节理和团粒结构,见根孔
	2.0~3.7	浅黄色砂黄土,垂直解理发育,颗粒较细(极细砂—细砂)
	3.7~4.6	浅黄色细砂层,质地较松软,地形上为缓坡
	4.6~6.5	浅黄色砂黄土,4.6~6.0 m,质地较硬,垂直节理发育,颗粒较细(极细砂);6.0~6.5 m,质地较松软,颗粒为细砂
	6.5~7.5	浅黄色(偏白)细砂层,有黄褐色铁染,未见底,在6.7 m处有一直径约5 cm的砍砸器
	未见底	

2 研究方法

2.1 光释光测年方法

在暗室中去除光释光样品不锈钢管两端2~3 cm可能曝光的部分用以进行环境剂量率和含水量的测试。用10%的盐酸(HCl)和30%的过氧化氢(H₂O₂)分别彻底去除样品中的碳酸盐和有机质,湿筛法提取出粒径范围在90~125 μm的颗粒,用40%的氢氟酸(HF)溶蚀40 min除去样品中的长石组分,得到纯净的石英颗粒。对提纯后的石英颗粒进行红外(IR)检验,若IRSL信号微弱(IRSL/OSL<10%)或几乎为本底值,则表明石英矿物中的长石颗粒去除的较彻底,可以进行样品等效剂量(De)的测试。等效剂量测试在陕西师范大学地理科学与旅游学院TL/OSL测年

实验室,利用Risø TL/OSL-DA-20型全自动释光仪进行测试,辐射源为⁹⁰Sr/⁹⁰Y型β源,蓝光激发光源波长为470±30 nm,滤光片为HoyaU-340,光电倍增管为EMI9235QB15。

环境剂量率主要由周围环境的U、Th、K等放射性元素含量及宇宙射线产生的放射性剂量和含水量决定^[30]。本文光释光样品U、Th、K的含量由中国地质调查局西安地质调查中心采用iCAP7400型全谱直读等离子光谱仪和iCAP RQ型电感耦合等离子体质谱仪测得。宇宙射线对剂量率值的贡献是依据采样点的经纬度、海拔高度、埋藏深度等并通过相关公式计算获得^[31]。含水量根据实验室实测含水量及沙地地层含水量校正,误差为10%^[32]。

2.2 粒度测试方法

称取约1.2 g样品自然风干或低温烘干,用10 mL浓度为10%的过氧化氢(H_2O_2)和盐酸(HCL)彻底除去有机质与碳酸盐。将处理好的样品反复洗至中性后,加入0.05 mol/L的六偏磷酸钠($(NaPO_3)_6$)溶液,放入超声波震荡仪中震荡10 min,使样品充分分散^[33]。粒度测试在陕西师范大学地理科学与旅游学院环境变迁实验室使用Mastersizer-2000型激光粒度仪进行测试。

2.3 石英表面微形态测试方法

称取5 g样品于烧杯中,依次加入20 mL的盐酸(30%)、过氧化氢(30%)和氯化亚锡($SnCl_2$)溶液,加热煮沸至碳酸盐、有机质和氧化铁等物质彻底除去。将处理好的样品放入烘箱中烘干,在双目镜下从每个样品中随机挑出20~30颗石英颗粒,均匀的粘贴在导电胶上,喷金后在扫描电镜下进行微形态测试^[34]。石英表面微形态测试在陕西师范大学地理科学与旅游学院环境变迁实验室使用MOTIC SMZ-168体视显微镜和MLA650F型矿物解离分析仪进行。

3 光释光年代测定

准确获得样品的等效剂量(De)值是获取可靠年龄结果的前提。等效剂量采用单片再生剂量法(SAR)测定^[35],该方法被广泛应用于第四纪沉积物年代测定。利用单片再生剂量法获取可靠年龄首先要确定测试条件。LQS剖面沉积相从顶部到底部分别为砂质古土壤、湖相砂、砂黄土,分别从砂质古土壤、湖相砂中选取代表性样品LQS-1和LQS-3进行测试条件的确定。

3.1 预热坪区

预热可以排空石英晶体浅陷阱中的热不稳定电子,获得稳定光敏的陷获电子,预热坪区实验目的是确定最适宜的预热温度^[36]。在预热坪区实验中,预热温度以20 °C为间隔从180 °C逐步升至300 °C,预热时间为10 s,每个温度测试3个样片,共计21个样片。实验结果表明(图3a,c):LQS-1、LQS-3分别在220 °C~260 °C、240 °C~300 °C之间出现一个温度坪区,此坪区内 De 值分别在11.13~11.38 Gy、23.49~24.48 Gy之间,不随温度的升高而发生明显变化。因此,坪区中任何一个温度都可以用于等效剂量值的测试。

3.2 剂量恢复和循环比

为了进一步检验预热坪区内的温度是否适合等效剂量的确定,还需进行剂量恢复(Dose Recovery)实验。测试时先将样品LQS-1和LQS-3蓝光激发完全晒退,之后给样品辐照一个近似于等效剂量的人工剂量,利用SAR法测得实测剂量,通过实测剂量与人工辐照剂量之比—恢复系数来衡量两者的差异。实验结果表明(图3b,d):LQS-1、LQS-3的预热温度在180 °C~280 °C、180 °C~300 °C之间时,恢复系数变化范围为0.96~1.01、0.98~1.05。样品的恢复系数均介于0.9~1.1,说明LQS-1样品选择180 °C~280 °C、LQS-3样品选择180 °C~300 °C作为SAR测试条件比较合适。

由于石英释光信号的灵敏度受反复的预热、 β 源的辐照和激发光源晒退而发生感量变化,因此需要对感量变化进行校正。感量变化校正的结果用循环比表示,若样品的循环比在0.9~1.1之间,说明样品中石英的感量变化得到了理想的校正。实验结果表明(图3b,d):LQS-1、LQS-3的预热温度在180 °C~300 °C、240 °C~300 °C之间时,循环比变化范围为0.92~1.09、1.02~1.06。综合预热坪区实验、剂量恢复实验和循环比实验,考虑合理的误差范围,最终选择Pre-heat 260 °C和Cut-heat 220 °C作为LQS-1和LQS-3的等效剂量值的测试条件。

3.3 光释光信号曲线特征

以LQS-3(湖相砂)和BLS-2(砂质古土壤)的晒退曲线和生长曲线为例进行释光特征分析。如图4显示,由蓝光激发的自然释光信号在2 s左右晒退至本底,晒退速率快,说明石英的释光信号以快速组分为主^[37-38]。并且校正后的释光信号随着再生剂量的增加而增加,生长曲线未达到饱和状态,因此LQS-3和BLS-2可通过内插方式得到可靠的等效剂量值。

3.4 光释光信号晒退程度分析

样品最后一次被埋藏前是否完全晒退是获得可靠年龄数据的前提。理论上晒退较好的样品校正后自然光释光信号强度的离散度(RSD_{N-OSL})应与校正后第一个再生剂量的光释光信号强度(RSD_{R1-OSL})的离散度相近^[39-40]。样品 De 的分布情况也能反映样品在最后一次被埋藏前的晒退情况,当 De 分布比较集中,离散度较小,说明样品晒退彻底; De 离散度大,说明样品最后一次被埋藏前晒退不好。从LQS和BLS

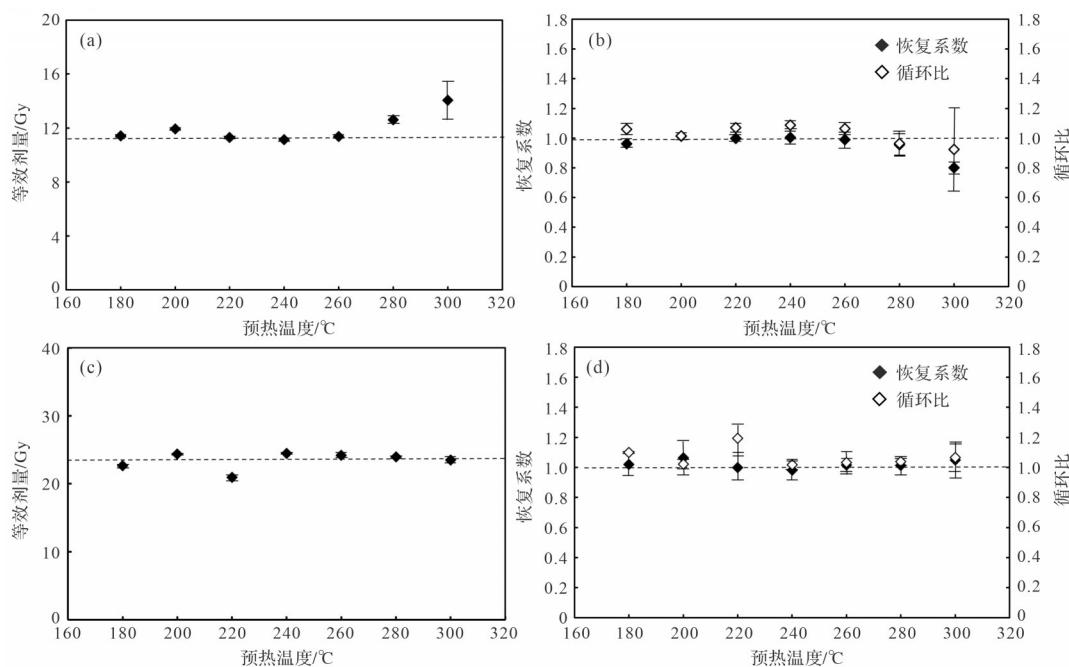


图3 石英矿物样品的预热坪区、剂量恢复和循环比实验

(a,b)LQS-1;(c,d)LQS-3

Fig.3 Preheat plateau plot dose recovery, and recycling ratio of quartz samples were tested

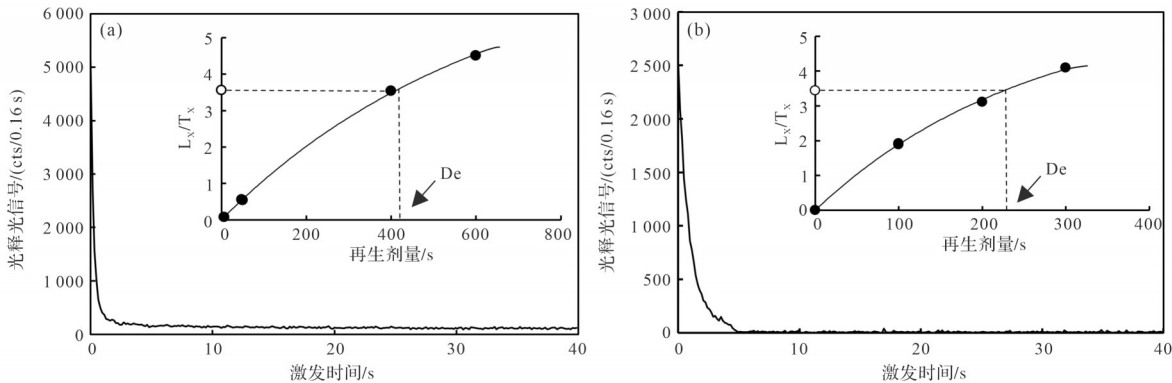


图4 石英矿物样品的释光信号晒退曲线及生长曲线

(a)LQS-3;(b)BLS-2

Fig.4 Optical simulated luminescence (OSL) bleaching curves and fitting growth curves of quartz samples were tested

两个剖面中选取样品LQS-3(湖相砂)和BLS-3(砂质古土壤)进行晒退程度分析(图5)。结果表明,LQS-3的 RSD_{N-OSL} 和 RSD_{R1-OSL} 分别为10.59%和8.72%,BLS-3的 RSD_{N-OSL} 和 RSD_{R1-OSL} 分别为19.60%和15.85%, RSD_{N-OSL} 和 RSD_{R1-OSL} 的离散度差值分别为1.87%和3.75%,离散度值较为接近。其中,样品LQS-3位于2 sigma置信区间的测片占88.9%,De的离散度为8.93%,等效剂量分布较为集中且呈正态分布(图5a,c),说明样品LQS-3在最后一次沉积埋藏前可能经历了充分晒退。而样品BLS-3位于2 sigma置信区间的测片占63.3%,De的离散度为21.46%,等效剂量

离散度较大(图5b,d),说明在最后一次沉积埋藏前可能晒退不彻底。

为了进一步得到准确的测年结果,分别使用平均年龄模型(Average Age Model, AAM)、中值年龄模型(Central Age Model, CAM)和最小年龄模型(Minimum Age Model, MAM)计算样品的等效剂量^[41-42]。LQS-3三种年龄模型计算所得的等效剂量分别为 25.14 ± 0.73 Gy(AAM)、 25.14 ± 0.75 Gy(CAM)、 25.14 ± 1.53 Gy(MAM),在误差范围内几乎相等。BLS-3三种年龄模型计算所得的等效剂量分别为 32.54 ± 1.32 Gy(AAM)、 32.05 ± 1.33 Gy(CAM)、 $25.69\pm$

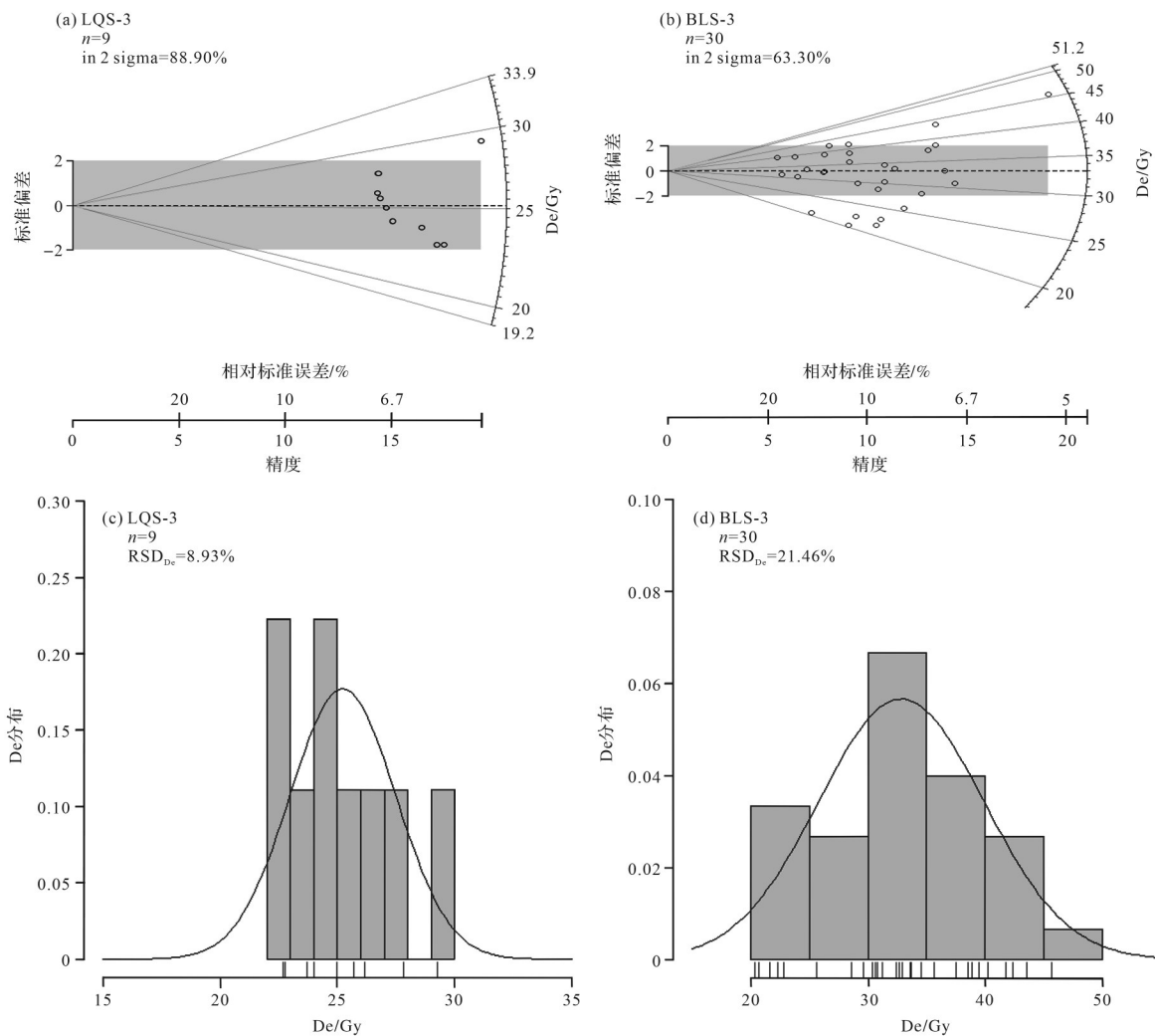


图5 样品LQS-3和BLS-3的De值分布放射图(a,b)与校正后的自然OSL信号相关关系与频率分布图(c,d)

Fig.5 Radial plots of De values (a, b) and corrected OSL and frequency distribution of De (c, d) of samples LQS-3 and BLS-3

1.95 Gy(MAM),最小年龄模型的等效剂量明显小于其他两种模型。所以,LQS-3在沉积埋藏前经历了较为充分的晒退,选取平均年龄模型计算最终年龄;BLS-3在沉积埋藏前可能未经历充分晒退,选择最小年龄模型计算其最终年龄。

4 结果

4.1 光释光年龄

利用Durcan *et al.*^[43]提出的剂量率和年龄计算器(DRAC)程序,并结合含水量、环境剂量率、海拔、经度等数据计算获得的浑善达克沙地LQS和BLS剖面的光释光年龄误差均小于10%。浑善达克沙地LQS、BLS剖面的测年结果表明(表2),LQS剖面OSL年龄范围为 $62.87\pm4.13\sim2.95\pm0.13$ ka; BLS剖面的

OSL年龄范围为 $17.80\pm1.10\sim1.00\pm0.10$ ka。两剖面光释光样品年龄整体上随深度的增加逐渐增大,符合地层堆积的规律,以此建立了两个剖面末次冰期以来的地层年代框架。

4.2 沉积物的粒度分布特征

沉积物的粒度主要受物源、搬运动力和沉积环境等因素的控制,不同的搬运动力和沉积环境使得沉积物粒度具有不同的组合形式,是研究古气候、古环境演变的重要替代性指标^[44]。LQS剖面粒度整体偏粗,呈单峰或双峰形态(图6a)。顶部砂质古土壤平均粒径介于 $359.13\sim391.77\mu\text{m}$,中值粒径介于 $379.1\sim381.5\mu\text{m}$ 。粒度组成与下伏湖相沉积类似,细颗粒含量增多,说明砂质古土壤可能是在湖相沉积的基础上受到气候变化的影响逐渐发育而来,也可能是由风成

表2 浑善达克沙地LQS、BLS剖面OSL测年结果

Table 2 OSL dating results of LQS and BLS profiles in the Otindag sandy land

样品编号	深度/m	沉积类型	$U/(\mu\text{g/g})$	$\text{Th}/(\mu\text{g/g})$	K/%	含水量/%	宇宙射线辐射剂量/(Gy/ka)	年剂量/(Gy/ka)	等效剂量/Gy	OSL年龄/ka
LQS-1	0.3	砂质土	0.83±0.20	3.14±0.43	1.63±0.04	0.52±0.05	0.25±0.03	2.44±0.07	7.20±0.26	2.95±0.13
LQS-2	1.2	砂质土	0.58±0.20	2.27±0.40	1.77±0.04	0.67±0.07	0.20±0.02	2.46±0.07	21.96±1.04	8.94±0.49
LQS-3	1.4	湖相砂	0.42±0.20	2.09±0.38	1.75±0.04	0.27±0.03	0.19±0.02	2.39±0.07	25.14±0.73	10.50±0.42
LQS-4	4.5	湖相砂	0.58±0.20	3.47±0.42	2.22±0.04	4.25±0.43	0.12±0.01	2.88±0.07	28.24±1.44	9.82±0.55
LQS-5	5.9	砂黄土	0.54±0.20	2.99±0.41	2.08±0.04	3.21±0.32	0.09±0.01	2.74±0.07	172.04±10.52	62.87±4.13
BLS-1	0.3	砂质土	0.40±0.05	1.40±0.02	2.03±0.02	1.05±0.11	0.23±0.02	2.37±0.04	2.39±0.09	1.00±0.10
BLS-2	0.9	砂质土	1.40±0.02	5.50±0.07	2.19±0.03	1.47±0.15	0.20±0.02	3.09±0.04	23.18±1.34	7.50±0.40
BLS-3	1.8	砂质土	1.20±0.01	3.70±0.04	2.24±0.03	1.51±0.15	0.17±0.02	3.13±0.05	25.69±1.95	8.20±0.64
BLS-4	2.1	砂黄土	1.00±0.01	3.10±0.04	2.09±0.03	2.34±0.23	0.16±0.02	2.66±0.04	32.30±2.12	12.20±0.80
BLS-5	3.6	砂黄土	0.30±0.04	3.40±0.04	2.02±0.02	1.31±0.13	0.13±0.01	2.43±0.03	37.40±3.17	15.40±1.30
BLS-6	4.0	风成砂	0.80±0.01	2.00±0.02	2.03±0.02	1.93±0.19	0.12±0.01	2.40±0.04	37.40±3.17	15.90±1.00
BLS-7	4.7	砂黄土	0.50±0.01	2.90±0.03	1.91±0.02	0.98±0.10	0.11±0.01	2.33±0.03	37.40±3.17	19.20±1.30
BLS-8	5.9	砂黄土	1.40±0.02	4.30±0.05	1.87±0.02	2.17±0.22	0.09±0.01	2.58±0.03	37.40±3.17	17.00±1.00
BLS-9	6.2	砂黄土	0.60±0.01	0.80±0.01	2.05±0.03	0.55±0.06	0.09±0.01	2.33±0.03	37.40±3.17	17.70±1.20
BLS-10	6.7	风成砂	0.50±0.01	0.60±0.01	2.16±0.03	0.80±0.08	0.08±0.01	2.38±0.03	37.40±3.17	17.80±1.10

砂夹积而形成;湖相砂平均粒径介于 202.03~374.43 μm ,中值粒径介于 186.0~357.9 μm 。其中 LQS-3 的粒度频率曲线呈尖而窄的单峰分布特征,粒径较粗。LQS-4 的粒度频率曲线呈双峰分布特征,细粒组分与入湖沉降的风成砂组分类似^[45],粗粒组分与近湖滨相沉积物组分类似^[46]。不同层位的湖相砂粒径差异较大,可能是由于早期湖泊面积较大,湖泊水位较高,接近湖心位置的水动力较小,沉积在底部的颗粒较细,而后期湖泊面积减小,湖滨水动力较大,携带湖岸粗颗粒沉降于湖泊中^[47];底部砂黄土的平均粒径为 256.4 μm ,中值粒径为 227.7 μm ,粒度频率分布曲线呈宽而缓的单峰分布特征,沉积动力较为复杂。

BLS 剖面粒度较 LQS 剖面偏细,呈单峰或多峰形态(图 6b),为风成沉积。顶部砂质古土壤的平均粒径为 86.48~129.20 μm ,中值粒径介于 89.14~114.34 μm ,大于 63 μm 的颗粒含量介于 67.97%~83.38%;砂黄土主要呈单峰和多峰分布,平均粒径范围为 85.68~166 μm ,中值粒径范围为 82.89~143.03 μm ,大于 63 μm 的颗粒含量介于 63.32%~89.69%;风成砂平均粒径范围为 140.55~166.56 μm ,中值粒径范围为 126.44~139.41 μm ,大于 63 μm 的颗粒含量超过 87%。砂质古土壤、砂黄土和风成砂的粒度频率分布曲线均存在相似的尖窄主峰和低矮的次峰,说明三者可能具有相似的搬运动力。

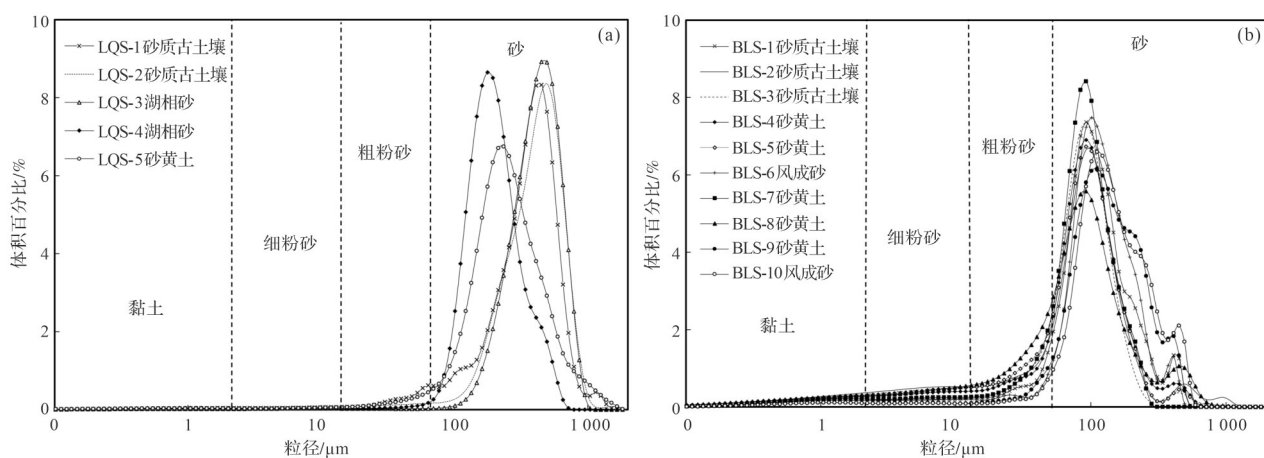


图6 LQS 和 BLS 剖面粒度频率分布曲线

Fig.6 Features of grain-size distribution frequency for the LQS and BLS profiles

4.3 湖相石英砂表面形态特征

在地表过程相对复杂的区域,沉积物不只受单一动力改造,仅凭沉积物粒度分布特征很难准确地判断其成因及沉积环境。由于石英硬度大、化学性质稳定,其表面形态特征能很好地反映搬运动力和沉积环境。因此,通过扫描电镜研究沉积物石英颗粒表面形态特征是分析沉积环境行之有效的方法。

扫描电镜结果显示(图7),LQS剖面中湖相石英砂呈次圆或者次棱角状,少数呈现磨圆度极好的球状(图7a),其表面存在碟形坑(D)、新月形撞击坑(B)、凹面(CO)等较为明显的风力搬运特征^[48],说明湖相沉积物的来源可能为风沙入湖。高能水环境下相互撞击形成的三角形撞击坑(TD)、连续的贝壳状断口(C)、“V”形撞击坑(VD)、方向性“V”形坑(Ddp)^[49]、直曲沟(SG)^[50]等特征说明湖相沉积后期可能受到河流、湖滨等强水动力环境的改造,结合湖相砂下发育有水平层理的砾石粗砂层(图2),表明LQS湖相砂为河湖相沉积物与风成沉积物的混合物,受风力分选(风吹沙入湖)和河流的共同作用。此外,水下磨光面以及长而浅的擦痕(S)和无规则的浅刻痕覆盖于强水动力环境特征之上,指示其形成时间较晚且水动力较弱,水环境经历了由动荡至平静的演变过程。因此,湖相沉积物来源除风沙入湖外,也可能是风沙入河再被搬运入湖,或者是河流相砂直

接入湖,或者是由于湖滨的水动力较大,携带湖岸粗颗粒沉降于湖泊。

5 讨论

5.1 浑善达克沙地地层年代框架可靠性分析

准确可靠的沉积地层年代框架的建立是分析区域气候环境变化的关键基础。LQS剖面沉积序列自上而下为砂质古土壤—湖相砂—砂黄土,BLS剖面沉积序列自上而下为砂质古土壤—砂黄土—风成砂—砂黄土—风成砂。末次冰盛期以来($17.8 \pm 1.1 \sim 12.2 \pm 0.8$ ka),BLS剖面发育风成砂与砂黄土互层,反映了千年时间尺度的气候波动。周亚利等^[25]对浑善达克沙地沙丘—砂黄土剖面释光测年结果显示,在19.6~11.4 ka间,沙地广泛分布风成砂和砂黄土。浑善达克沙地东缘风成砂的沉积年龄为19.21~15.07 ka^[51]。同时期的沙层也在沙地东部浩来呼热剖面底部^[11]和沙地北部锡林浩特附近沙丘底部^[10,24]的地层中发现,均与本文测得的风成砂、砂黄土光释光年龄结果一致,表明测年结果较为可靠。

研究表明,北半球大部分地区在北大西洋9.4 ka B.P.冷事件和10.3 ka B.P.冷事件^[52]发生时,气候变冷、变干,风沙活动增加。LQS剖面湖相砂顶部和底部的年龄为 10.50 ± 0.42 ka和 9.82 ± 0.55 ka,在误差范围内湖

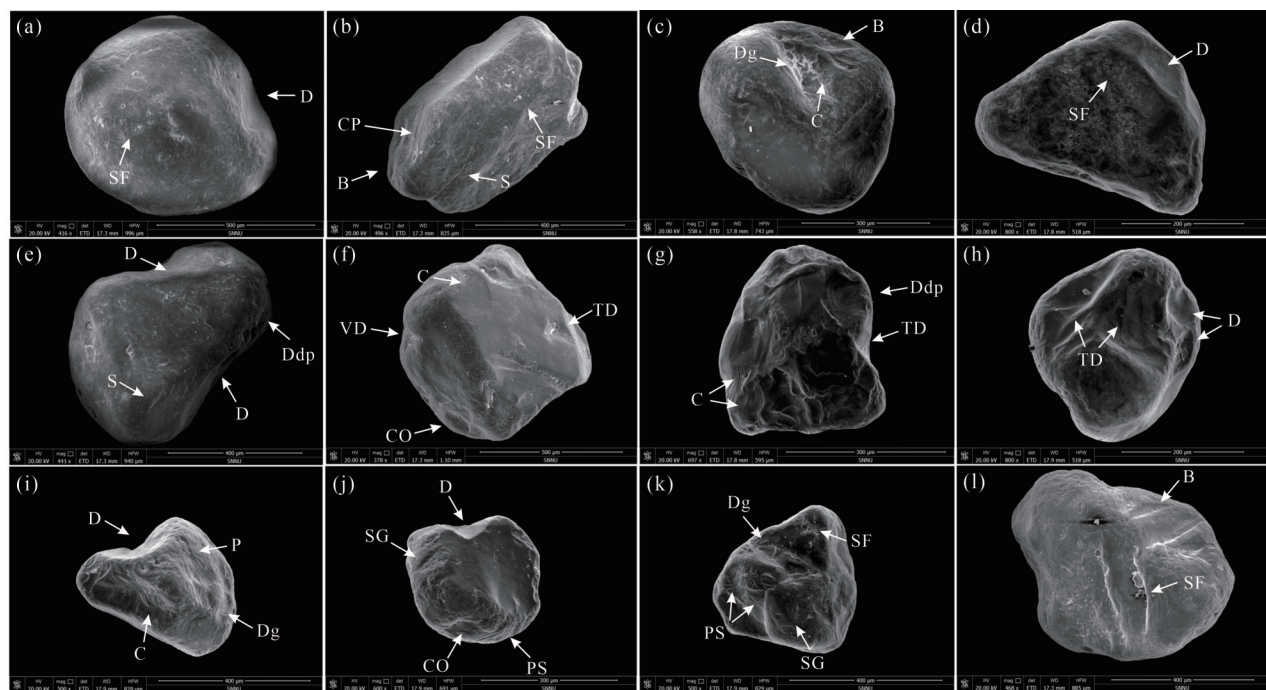


图7 LQS剖面湖相石英砂表面形态特征

Fig.7 Surface morphological characteristics of lacustrine quartz sand in profile LQS

相沉积的年龄几乎一致,说明在10 ka左右短暂存在过湖泊,湖泊的形成与消失可能与风沙活动相关。当沙丘在移动的过程中切断河流时,河水在丘间带聚集形成湖泊,而当后期沙丘再次移动时会导致湖水外泄,湖泊消失^[53]。在距今9.9~8.2 ka期间,贯穿沙地南北方向的多个固定一半固定沙丘和沙/黄土剖面发育厚层粗砂层^[13]。Mason *et al.*^[54]和Gong *et al.*^[27]在风成砂—古土壤序列底部测得10 ka左右发育的风成砂。沙地东北部山地斜坡也记录到了风成砂发育^[24]。以上关于风沙沉积的年龄记录与9.4 ka B.P.和10.3 ka B.P.两次冷事件相对应,该时期的湖相砂与风成砂为同期异相沉积物,风成砂的广泛发育说明在此时间段内风沙活动较为频繁。

LQS剖面砂质古土壤顶部和底部的年龄为2.95±0.13 ka、8.94±0.49 ka,BLS剖面砂质古土壤上、中、下部的年龄为1.00±0.10 ka、7.50±0.40 ka、8.20±0.64 ka。两剖面的砂质古土壤发育年龄在8.94±0.49~2.95±0.13 ka,1.00±0.10 ka,与区域内关于全新世的砂质古土壤测年结果一致^[55]。另外,HSHN(沙地北部)、MJZ(沙地东部)剖面古土壤的测年结果为8.72±0.16~0.71±0.03 ka,7.79±0.2~2.74±0.06 ka^[9]。沙地西部BN和SX剖面风成砂下部砂质古土壤的形成始于9.5±0.45 ka和10.1±0.45 ka,而分别结束于4.0±0.18 ka和3.3±0.15 ka^[56]。沙地南缘同一层位古土壤下界年龄为4.60±0.40 ka,沙地北缘CG-5087砂质古土壤顶部及CG-5088地表以下1.5 m处砂质古土壤的放射性¹⁴C年龄为2.82±0.12 cal. ka B.P.、2.08±0.19 cal. ka B.P.^[24]。以上研究结果表明,全新世中期浑善达克沙地广泛发育砂质古土壤。

5.2 末次盛冰期以来浑善达克沙地的气候变化

浑善达克沙地南缘两个沉积序列记录了该区域环境的演化过程。末次盛冰期时期,太阳辐射达到最小值^[57],北极冰盖增加,东亚冬季风增强,沙地南部主要发育风成砂与砂黄土,气候寒冷干燥,风沙活动强烈。17.8~17.0 ka发育的风成砂与砂黄土表征着末次盛冰期干冷的气候环境。同时期,浑善达克沙地面积扩张了37%^[25],中国季风区西北缘的腾格里沙漠、巴丹吉林沙漠以及共和沙地的面积也相应地扩大了19.8%~39.0%^[58],青藏高原东北部湖泊因气候寒冷干燥而处于干涸状况^[59],新疆阿尔泰山冰川也发生大规模前进^[60]。末次冰消期时期,太阳辐射增强,东亚冬季风减弱,气候向暖湿过渡。15.9 ka和12.2 ka

发育的风成砂(BLS-6)和砂黄土(BLS-4)较好的对应了末次冰消期气温回暖过程中H1(Heinrich 1)和YD(Younger Dryas)两次明显的降温减湿事件,在格陵兰冰芯^[61]、董哥洞^[62]和葫芦洞^[63,64]石笋及赤铁矿染色颗粒含量^[65](图8)中均有记录,据此认为这两个气候突变事件具有全球性和普遍性。

全新世气候不稳定,存在明显的气候波动和快速变化^[66,67]。全新世早期,LQS剖面在10 ka左右发育湖相粗砂层,湖相砂与风成砂为同期异相沉积物,是不同地貌部位对地表过程的不同响应,均指示冷干的气候环境,湖泊的发育与9.4 ka(冷事件6)和10.3 ka(冷事件7)的北大西洋冷事件相呼应(图8)。8.2 ka和8.94 ka发育的砂质古土壤指示了全新世早期沙地气候由冷干逐渐转为暖湿。哈根淖尔沉积记录显示,在10.8~9.5 cal. ka B.P.时期气候冷干,9.5~8.5 cal. ka B.P.气候暖湿、湖面扩张^[28]。浑善达克沙地风成砂/古土壤沉积物粒度^[26]、神农架大九湖泥炭沉积物的化学指标和孢粉记录^[68]及沙地浩来呼热古湖泊沉积物中硅藻化石^[69]的研究结果均表明全新世早期冬季风不断减弱,夏季风不断增强。沙地中部风成砂—古土壤剖面也再次证明了10 ka左右气候由冷干向暖湿过渡^[70]。

全新世适宜期(8.20~2.95 ka)^[71],BLS和LQS发育灰黑色砂质古土壤,堆积速率较风成砂和砂黄土慢,粗颗粒含量减少,受太阳辐射和东亚夏季风增强的影响,气候较为温暖湿润,沙丘处于固定状态。此时期,中国北方沙漠/沙地古土壤年龄记录占比超过60%^[72],整个黄土高原黄土沉积减少,古土壤形成增加^[73],中国北方科尔沁沙地沙丘处于大幅度稳定阶段^[74],浑善达克沙地明显比现代湿润,古土壤较为发育^[56],沙丘活动减少^[75],此时的岱海、黄旗海也处于高湖面^[76,77]。但沙地气候并不是一直维持温暖湿润状态。周亚利等^[13]在浑善达克沙地发现光释光年龄为5.24 ka、4.97 ka、4.04 ka、3.32 ka的沙层,5.64~5.12 ka华北平原西部的孢粉^[78]以及公元前5 500年左右气候变化导致的新石器文化发生重大变化^[79]等证据表明气候在5 ka左右存在波动。全新世晚期,太阳辐射减弱,东亚冬季风增强,气候逐渐变干,风沙活动增加。浑善达克沙地风成沉积较为发育^[13,24],浩来呼热剖面在1.8 ka堆积有砂黄土^[11],指示了偏干的气候环境。BLS剖面发育1 ka左右的砂质古土壤与0.98~0.73 ka岱海深水沉积剖面下发育的粉砂质黏

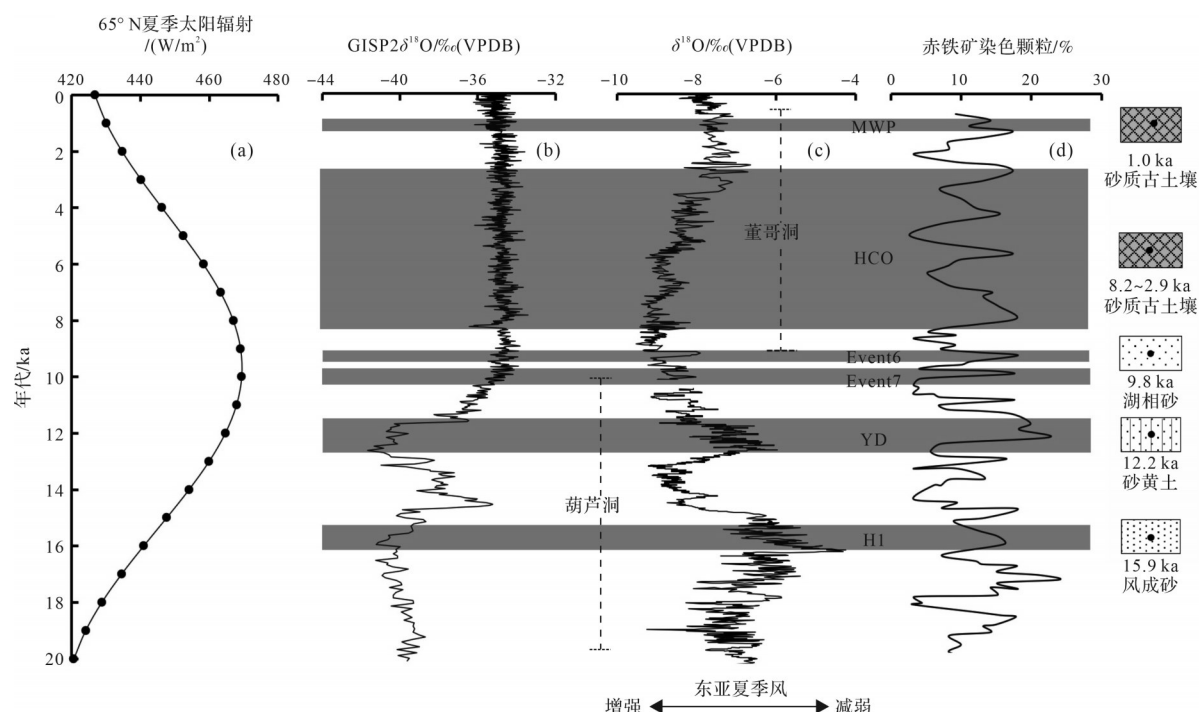


图8 浑善达克沙地记录与其他区域古气候记录对比

(a) 65° N 夏季太阳辐射能量曲线^[57]; (b) 格陵兰 GRIP2 冰芯 $\delta^{18}\text{O}$ 记录^[61]; (c) 董哥洞^[62]和葫芦洞^[63-64]石笋 $\delta^{18}\text{O}$ 记录; (d) VM 29-291 和 VM 23-81 岩心赤铁矿染色颗粒含量组合记录^[65]

Fig.8 Comparison of the record of samples from the Otindag sandy land with paleoclimate records from other regions

(a) average summer insolation for 65° N^[57]; (b) Greenland GRIP2 ice core $\delta^{18}\text{O}$ record^[61]; (c) Dongge cave^[62] and Hulu Cave^[63-64] $\delta^{18}\text{O}$ records; (d) hematite-stained grains are from the composite VM 29-191 and VM 23-81 record^[65]

土^[80], 均指示了温暖湿润的气候条件, 与全球范围内广泛出现的中世纪暖期(Medieval Warm Period, MWP)相一致^[81], 是全新世晚期整体较干冷气候背景下暖湿时段的体现。

6 结论

(1) 末次盛冰期以来至全新世(18.0~11.5 ka), 沙地主要发育风成砂与砂黄土, 受太阳辐射及东亚冬季风较强的影响, 气候较为冷干, 风沙活动强烈, 存在千年尺度冷暖干湿变化。全新世早期(11.5~8.2 ka), 太阳辐射和东亚夏季风逐渐增强, 温度波动上升, 气候相对干冷, 多发育沙层, 局部也有砂质古土壤发育。全新世适宜期(8.2~2.7 ka), 太阳辐射达到最大值, 东亚夏季风强盛, 气候最为温暖湿润, 两剖面均发育砂质古土壤。全新世晚期(2.7 ka 至今), 太阳辐射减弱, 东亚冬季风逐渐增强, 风沙活动增加, 气候较全新世适宜期恶化, 整体上温和偏干。

(2) LQS 剖面湖相沉积物的形成主要受局地地

貌的影响, 类似于现代沙地沙丘与湖泊并存, 反映干冷的气候环境。湖相沉积物沉积过程较为复杂, 受风力、河流、湖泊三种沉积动力的共同影响。

致谢 非常感谢两位审稿专家和编辑部老师提出的建设性修改意见。

参考文献(Reference)

- [1] Huang J P, Yu H P, Dai A G, et al. Drylands face potential threat under 2 °C global warming target[J]. Nature Climate Change, 2017, 7(6): 417-422.
- [2] 李明启, 靳鹤龄, 张洪, 等. 浑善达克沙地磁化率和有机质揭示的全新世气候变化[J]. 沉积学报, 2005, 23(4): 683-689.
[Li Mingqi, Jin Heling, Zhang Hong, et al. Climate change revealed by magnetic susceptibility and organic matter during the Holocene in Hunshandake Desert[J]. Acta Sedimentologica Sinica, 2005, 23(4): 683-689.]
- [3] Ming G D, Zhou W J, Wang H, et al. Moisture variations in lacustrine-eolian sequence from the Hunshandake sandy land associated with the East Asian Summer Monsoon changes since the Late Pleistocene[J]. Quaternary Science Reviews, 2020, 233: 106210.
- [4] Zhou Y W, Han Z Y, Li X S, et al. Sandy loess records

- of precipitation changes and monsoon migrations in the Hunshandake sandy land since the Last Glacial Maximum[J]. *Paleoceanography and Paleoclimatology*, 2018, 33(9): 945-957.
- [5] Goldsmith Y, Broecker W S, Xu H, et al. Northward extent of East Asian monsoon covaries with intensity on orbital and millennial timescales[J]. *Proceedings of the National Academy of Sciences of the United States of America*, 2017, 114(8): 1817-1821.
- [6] Xiao J L, Si B, Zhai D Y, et al. Hydrology of Dali lake in central-eastern Inner Mongolia and Holocene East Asian monsoon variability[J]. *Journal of Paleolimnology*, 2008, 40(1): 519-528.
- [7] 姜雅娟,王维,马玉贞,等. 内蒙古鄂尔多斯高原泊江海子全新世气候变化初步研究[J]. 第四纪研究,2014,34(3):654-665. [Jiang Yajuan, Wang Wei, Ma Yuzhen, et al. A preliminary study on Holocene climate change of Ordos Plateau, as inferred by sedimentary record from Bojianghaizi Lake of Inner Mongolia, China[J]. *Quaternary Sciences*, 2014, 34(3): 654-665.]
- [8] Fan J W, Xiao J L, Wen R L, et al. Carbon and nitrogen signatures of sedimentary organic matter from Dali Lake in Inner Mongolia: Implications for Holocene hydrological and ecological variations in the East Asian summer monsoon margin[J]. *Quaternary International*, 2017, 452: 65-78.
- [9] 周亚利,鹿化煜,张家富,等. 高精度光释光测年揭示的晚第四纪毛乌素和浑善达克沙地沙丘的固定与活化过程[J]. 中国沙漠,2005,25(3):342-350. [Zhou Yali, Lu Huayu, Zhang Jiafu, et al. Active and inactive phases of sand-dune in Mu Us and Otindag sandlands during Late Quaternary suggested by OSL Dating[J]. *Journal of Desert Research*, 2005, 25(3): 342-350.]
- [10] 斯鹤龄,苏志珠,孙良英,等. 浑善达克沙地全新世气候变化[J]. 科学通报,2004,49(15):1532-1536. [Jin Heling, Su Zhizhu, Sun Liangying, et al. Holocene climatic change in Hunshandake desert[J]. *Chinese Science Bulletin*, 2004, 49 (15): 1532-1536.]
- [11] 刘瑾,王永,姚培毅,等. 末次冰消期以来内蒙古东部气候变化:基于风成砂—古土壤序列的地球化学记录[J]. 中国地质,2015,42(4):1103-1114. [Liu Jin, Wang Yong, Yao Peiyi, et al. A study of paleoclimate changes in east Inner Mongolia since the Last deglaciation on the basis of Aeolian sand-paleosoil series geochemical records[J]. *Geology in China*, 2015, 42(4): 1103-1114.]
- [12] 李森,孙武,李孝泽,等. 浑善达克沙地全新世沉积特征与环境演变[J]. 中国沙漠,1995,15(4):323-331. [Li Sen, Sun Wu, Li Xiaoze, et al. Sedimentary characteristics and environmental evolution of Otindag sandy land in Holocene[J]. *Journal of Desert Research*, 1995, 15(4): 323-331.]
- [13] 周亚利,鹿化煜,Mason J A,等. 浑善达克沙地的光释光年代序列与全新世气候变化[J]. 中国科学:地球科学,2008,38(4):452-462. [Zhou Yali, Lu Huayu, Mason J A, et al. Optically stimulated luminescence dating of Aeolian sand in the Otindag dune field and Holocene climate change[J]. *Science China Earth Sciences*, 2008, 38(4): 452-462.]
- [14] Lancaster N, Yang X P, Thomas D. Spatial and temporal complexity in Quaternary desert datasets: Implications for interpreting past dryland dynamics and understanding potential future changes[J]. *Quaternary Science Reviews*, 2013, 78: 301-302.
- [15] Zhang Z S. Research resource review: Climate change in deserts: Past, present and future[J]. *Progress in Physical Geography: Earth and Environment*, 2016, 40(1): 181-183.
- [16] 凌智永,李志忠,罗磊,等. 关于沙漠环境演变几种研究指标的探讨[J]. 云南地理环境研究,2009,21(2):86-91. [Ling Zhiyong, Li Zhizhong, Luo Lei, et al. The discussion about the several research indicators of the desert environment evolution[J]. *Yunnan Geographic Environment Research*, 2009, 21(2): 86-91.]
- [17] Song Y G, Lai Z P, Li Y, et al. Comparison between luminescence and radiocarbon dating of Late Quaternary loess from the Ili Basin in Central Asia[J]. *Quaternary Geochronology*, 2015, 30: 405-410.
- [18] Stokes S, Thomas D S G, Washington R. Multiple episodes of aridity in southern Africa since the last interglacial Period[J]. *Nature*, 1997, 388(6638): 154-158.
- [19] Lancaster N, Kocurek G, Singhvi A, et al. Late Pleistocene and Holocene dune activity and wind regimes in the western Sahara Desert of Mauritania[J]. *Geology*, 2002, 30(11): 991-994.
- [20] Moska P, Murray A S, Bluszcz A. Luminescence properties of single grain quartz to determine the history of a sample from the Sahara Desert[J]. *Quaternary Geochronology*, 2010, 5(2/3): 96-101.
- [21] Li G Q, Li F L, Jin M, et al. Late Quaternary lake evolution in the Gaxun Nur Basin, central Gobi Desert, China, based on quartz OSL and K-feldspar pIRIR dating of paleoshorelines[J]. *Journal of Quaternary Science*, 2017, 32(3): 347-361.
- [22] 春喜,陈发虎,范育新,等. 乌兰布和沙漠腹地古湖存在的沙嘴证据及环境意义[J]. 地理学报,2009,64(3):339-348. [Chun Xi, Chen Fahu, Fan Yuxin, et al. Evidence of palaeo-lake existence in Ulan Buh desert and its environmental evolution[J]. *Acta Geographica Sinica*, 2009, 64(3): 339-348.]
- [23] Richter D, Krötschek M. A new thermoluminescence dating technique for heated flint[J]. *Archaeometry*, 2006, 48(4): 695-705.
- [24] Yang X, Zhu B, Wang X, et al. Late Quaternary environmental changes and organic carbon density in the Hunshandake sandy land, eastern Inner Mongolia, China[J]. *Global and Planetary Change*, 2008, 61(1/2): 70-78.
- [25] 周亚利,鹿化煜,张小艳,等. 末次盛冰期和全新世大暖期浑善达克沙地边界的变化[J]. 第四纪研究,2013,33(2):228-242. [Zhou Yali, Lu Huayu, Zhang Xiaoyan, et al. Changes of the border of Otindag sand field (northern China) during the

- Last Glacial Maximum and Holocene Optimum[J]. Quaternary Sciences, 2013, 33(2): 228-242.]
- [26] 张洪,靳鹤龄,苏志珠,等. 全新世浑善达克沙地粒度旋回及其反映的气候变化[J]. 中国沙漠, 2005, 25 (1) : 1-7. [Zhang Hong, Jin Heling, Su Zhizhu, et al. Climate changes revealed by grain-size cycles of Holocene in Hunshandake desert[J]. Journal of Desert Research, 2005, 25(1): 1-7.]]
- [27] Gong Z J, Li S H, Sun J M, et al. Environmental changes in Hunshandake (Otindag) sandy land revealed by optical dating and multi-proxy study of dune sands[J]. Journal of Asian Earth Sciences, 2013, 76: 30-36.
- [28] 黄世鑫,春喜,梁文军,等. 浑善达克沙地早全新世气候变化[J]. 干旱区资源与环境, 2018, 32 (8) : 114-121. [Huang Shixin, Chun Xi, Liang Wenjun, et al. Climate change in Otindag sandy land during the Early Holocene[J]. Journal of Arid Land Resources and Environment, 2018, 32(8): 114-121.]]
- [29] 蒋凯. 13万年以来浑善达克沙地南缘黄土—古土壤序列的环境磁学和地球化学研究[D]. 北京: 中国地质科学院, 2018. [Jiang Kai. Environmental magnetic and geochemical characteristics of a Late Pleistocene loess-paleosol sequence in the southern Hunshandake sandy land[D]. Beijing: Chinese Academy of Geological Sciences, 2018.]
- [30] 米小建,周亚利. 光释光测年及发展[J]. 湛江师范学院学报, 2012, 33 (6) : 66-70. [Mi Xiaojian, Zhou Yali. Optical dating method and its development[J]. Journal of Zhanjiang Normal University, 2012, 33(6): 66-70.]
- [31] Prescott J R, Hutton J T. Cosmic ray contributions to dose rates for luminescence and ESR dating: Large depths and long-term time variations[J]. Radiation Measurements, 1994, 23(2/3): 497-500.
- [32] 孙晓巍. 浑善达克沙地中更新世以来的光释光年代学研究[D]. 西安: 陕西师范大学, 2019. [Sun Xiaowei. Optically stimulated luminescence geochronology of Hunshandake sandy land since Middle Pleistocene[D]. Xi'an: Shaanxi Normal University, 2019.]
- [33] 鹿化煜,安芷生. 黄土高原黄土粒度组成的古气候意义[J]. 中国科学: 地球科学, 1998, 28 (3) : 278-283. [Lu Huayu, An Zhisheng. Paleoclimatic significance of grain size of loess-palaeosol deposit in Chinese Loess Plateau[J]. Science China Earth Sciences, 1998, 28(3): 278-283.]
- [34] Chen R C, Chen J, Ma J X, et al. Quartz grain surface micro-textures of dam-break flood deposits from a landslide-dammed lake: A case study[J]. Sedimentary Geology, 2019, 383: 238-247.
- [35] Murray A, Arnold L J, Buylaert J P, et al. Optically stimulated luminescence dating using quartz[J]. Nature Reviews Methods Primers, 2021, 1(1): 72.
- [36] Murray A S, Wintle A G. Luminescence dating of quartz using an improved single-aliquot regenerative-dose protocol[J]. Radiation Measurements, 2000, 32(1): 57-73.
- [37] Singarayer J S, Bailey R M. Component-resolved bleaching spectra of quartz optically stimulated luminescence: Preliminary results and implications for dating[J]. Radiation Measurements, 2004, 38(1): 111-118.
- [38] 贾彬彬,周亚利,赵军. 新疆阿尔泰山东段冰碛物光释光测年研究[J]. 地理学报, 2018, 73 (5) : 957-972. [Jia Binbin, Zhou Yali, Zhao Jun. Optically stimulated luminescence dating of moraines in east Altay Mountains, Xinjiang[J]. Acta Geographica Sinica, 2018, 73(5): 957-972.]
- [39] 张家富,周力平,姚书春,等. 湖泊沉积物的¹⁴C和光释光测年: 以固城湖为例[J]. 第四纪研究, 2007, 27 (4) : 522-528. [Zhang Jiafu, Zhou Liping, Yao Shuchun, et al. Radiocarbon and optical dating of lacustrine sediments: A case study in lake Gucheng[J]. Quaternary Sciences, 2007, 27(4): 522-528.]
- [40] Zhang J F, Zhou L P, Yue S Y. Dating fluvial sediments by optically stimulated luminescence: Selection of equivalent doses for age calculation[J]. Quaternary Science Reviews, 2003, 22 (10/11/12/13): 1123-1129.
- [41] Galbraith R F, Roberts R G, Laslett G M, et al. Optical dating of single and multiple grains of quartz from Jimmum rock shelter, northern Australia: Part I, experimental design and statistical models[J]. Archaeometry, 1999, 41(2): 339-364.
- [42] Fan Y X, Li Z J, Cai Q S, et al. Dating of the Late Quaternary high lake levels in the Jilantai area, northwestern China, using optical luminescence of quartz and K-feldspar[J]. Journal of Asian Earth Sciences, 2022, 224: 105024.
- [43] Durcan J A, King G E, Duller G A T. DRAC: Dose Rate and Age Calculator for trapped charge dating[J]. Quaternary Geochronology, 2015, 28: 54-61.
- [44] 白敏,鲁瑞洁,丁之勇,等. 青海湖湖东沙地粒度端元分析及其指示意义[J]. 第四纪研究, 2020, 40 (5) : 1203-1215. [Bai Min, Lu Ruijie, Ding Zhiyong, et al. End-member analysis of grain-size in the east of Qinghai Lake and its environmental implications[J]. Quaternary Sciences, 2020, 40(5): 1203-1215.]
- [45] 乌日查呼,春喜,张卫青,等. 浑善达克沙地沙粒特征及其沉积环境[J]. 西北林学院学报, 2021, 36 (1) : 69-76. [Wuri Chahu, Chun Xi, Zhang Weiqing, et al. Grain size analysis and the sedimentary environment in Otindag sandy land[J]. Journal of Northwest Forestry University, 2021, 36(1): 69-76.]
- [46] 郭晓阳,王维,王国良,等. 季风边缘区湖泊表层沉积物粒度组分分布特征与影响因素[J]. 地理研究, 2016, 35 (4) : 677-691. [Guo Xiaoyang, Wang Wei, Wang Guoliang, et al. Within-lake distributions of grain-size components and environmental implications based on the survey of lake surface sediment of Chinese monsoon marginal area[J]. Geographical Research, 2016, 35(4): 677-691.]
- [47] 田飞,王永,袁路朋,等. 浑善达克沙地碱湖表层沉积物的粒度、沉积有机质变化特征与指示意义[J]. 地学前缘, 2022, 29 (2) : 317-326. [Tian Fei, Wang Yong, Yuan Lupeng,

- et al. Surface sediments of an alkaline lake in the Otindag sandy land: Grain size and sedimentary organic matter variations and their environmental significance[J]. *Earth Science Frontiers*, 2022, 29(2): 317-326.]
- [48] 谢又予. 中国石英砂表面结构特征图谱[M]. 北京:海洋出版社, 1984: 40-53. [Xie Youyu. *Atlas of quartz sand surface textural features of China micrographs*[M]. Beijing: China Ocean Press, 1984: 40-53.]
- [49] 郭红锋, 魏东岚, 张威. 基于SEM的辽南红色风化壳石英颗粒化学成因特征分析[J]. 第四纪研究, 2022, 42(6): 1613-1623. [Guo Hongfeng, Wei Donglan, Zhang Wei. Characterization of the chemical genesis of red weathered crust quartz grains in the southern Liaoning province based on SEM [J]. *Quaternary Sciences*, 2022, 42(6): 1613-1623.]
- [50] 江新胜, 徐金沙, 潘忠习. 鄂尔多斯盆地白垩纪沙漠石英沙颗粒表面特征[J]. 沉积学报, 2003, 21(3): 416-422. [Jiang Xinsheng, Xu Jinsha, Pan Zhongxi. Microscopic features on quartz sand grain surface in the Cretaceous Desert of Ordos Basin[J]. *Acta Sedimentologica Sinica*, 2003, 21(3): 416-422.]
- [51] 渠洪杰, 陈英富, 卢晶, 等. 浑善达克沙地最近一次大规模沙化的沉积记录及其光释光年龄[J]. 中国地质, 2022, 49(3): 1003-1004. [Qu Hongjie, Chen Yingfu, Lu Jing, et al. Sedimentary record and OSL age of the latest large-scale desertification in Otindag sandy land[J]. *Geology in China*, 2022, 49(3): 1003-1004.]
- [52] 王绍武. 全新世北大西洋冷事件:年代学和气候影响[J]. 第四纪研究, 2009, 29(6): 1146-1153. [Wang Shaowu. Holocene cold events in the North Atlantic: Chronology and climatic impact [J]. *Quaternary Sciences*, 2009, 29(6): 1146-1153.]
- [53] Loope D B, Swinehart J B, Mason J P. Dune-dammed paleovalleys of the Nebraska Sand Hills: Intrinsic versus climatic controls on the accumulation of lake and marsh sediments[J]. *GSA Bulletin*, 1995, 107(4): 396-406.
- [54] Mason J A, Lu H, Zhou Y, et al. Dune mobility and aridity at the desert margin of northern China at a time of peak monsoon strength[J]. *Geology*, 2009, 37(10): 947-950.
- [55] 杨利荣, 岳乐平. 浑善达克沙地末次冰期晚期到全新世的环境转型[J]. 地球环境学报, 2011, 2(1): 301-306. [Yang Lirong, Yue Leping. The environmental transformation from Late last glacial to Holocene of Otindag sandy land[J]. *Journal of Earth Environment*, 2011, 2(1): 301-306.]
- [56] 杨小平, 梁鹏, 张德国, 等. 中国东部沙漠/沙地全新世地层序列及其古环境[J]. 中国科学:地球科学, 2019, 49(8): 1293-1307. [Yang Xiaoping, Liang Peng, Zhang Deguo, et al. Holocene aeolian stratigraphic sequences in the eastern portion of the desert belt (sand seas and sandy lands) in northern China and their palaeoenvironmental implications[J]. *Science China Earth Sciences*, 2019, 49(8): 1293-1307.]
- [57] Berger A, Loutre M F. Insolation values for the climate of the last 10 million years[J]. *Quaternary Science Reviews*, 1991, 10(4): 297-317.
- [58] 冯晗, 鹿化煜, 戈双文, 等. 末次盛冰期和全新世大暖期中国季风区西北缘沙漠空间格局重建初探[J]. 第四纪研究, 2013, 33(2): 252-259. [Feng Han, Lu Huayu, Yi Shuangwen, et al. The border changes of the deserts/sand field in the East Asian Monsoon marginal region during the Last Glacial Maximum and Holocene Optimum[J]. *Quaternary Sciences*, 2013, 33(2): 252-259.]
- [59] 沈吉. 末次盛冰期以来中国湖泊时空演变及驱动机制研究综述:来自湖泊沉积的证据[J]. 科学通报, 2012, 57(34): 3228-3242. [Shen Ji. Spatiotemporal variations of Chinese lakes and their driving mechanisms since the Last Glacial Maximum: A review and synthesis of lacustrine sediment archives [J]. *Chinese Science Bulletin*, 2012, 57(34): 3228-3242.]
- [60] 江合理, 赵井东, 殷秀峰, 等. 阿尔泰山喀纳斯河流域末次冰期OSL年代学新证[J]. 冰川冻土, 2012, 34(2): 304-310. [Jiang Heli, Zhao Jingdong, Yin Xiufeng, et al. New OSL chronology of the Last Glaciation in Kanas River Valley, Altay Mountains, China[J]. *Journal of Glaciology and Geocryology*, 2012, 34(2): 304-310.]
- [61] Grootes P M, Stuiver M. GISP2 oxygen isotope data[DB/OL]. Pangaea, [1999-12-23]. <https://doi.org/10.1594/Pangaea.56094>.
- [62] Dykoski C A, Edwards R L, Cheng H, et al. A high-resolution, absolute-dated Holocene and deglacial Asian monsoon record from Dongge Cave, China[J]. *Earth and Planetary Science Letters*, 2005, 233(1/2): 71-86.
- [63] Wang Y J, Cheng H, Edwards R L, et al. A high-resolution absolute-dated Late Pleistocene monsoon record from Hulu Cave, China[J]. *Science*, 2001, 294(5550): 2345-2348.
- [64] 吴江滢, 汪永进, 程海, 等. 葫芦洞石笋记录的19.9-17.1ka BP东亚夏季风增强事件[J]. 中国科学:地球科学, 2009, 39(1): 61-69. [Wu Jiangying, Wang Yongjin, Cheng Hai, et al. An exceptionally strengthened East Asian summer monsoon event between 19.9 and 17.1 ka BP recorded in a Hulu stalagmite[J]. *Science China Earth Sciences*, 2009, 39(1): 61-69.]
- [65] Bond G, Showers W, Cheseby M, et al. A pervasive millennial-scale cycle in North Atlantic Holocene and glacial climates[J]. *Science*, 1997, 278(5341): 1257-1266.
- [66] Dansgaard W, Johnsen S J, Clausen H B, et al. Evidence for general instability of past climate from a 250-kyr ice-core record[J]. *Nature*, 1993, 364(6434): 218-220.
- [67] von Grafenstein U, Erlenkeuser H, Brauer A, et al. A mid-European decadal isotope-climate record from 15, 500 to 5000 years B. P. [J]. *Science*, 1999, 284(5420): 1654-1657.
- [68] Zhang H W, Cheng H, Spötl C, et al. A 200-year annually laminated stalagmite record of precipitation seasonality in south-eastern China and its linkages to ENSO and PDO[J]. *Scientific Reports*, 2018, 8(1): 12344.
- [69] 关友义, 王永, 姚培毅, 等. 内蒙古克什克腾旗浩来呼热古

- 湖泊全新世以来的环境演变[J]. 地质通报, 2010, 29(6): 891-900. [Guan Youyi, Wang Yong, Yao Peiyi, et al. Environmental evolution since the Holocene in the Haolaihure ancient lake, Keshiketengqi, Inner Mongolia, China[J]. Geological Bulletin of China, 2010, 29(6): 891-900.]
- [70] 韩鹏, 孙继敏. 浑善达克沙地的光释光测年研究[J]. 第四纪研究, 2004, 24(4): 480. [Han Peng, Sun Jimin. Optical dating of dune sands in the Hunshandake desert[J]. Quaternary Sciences, 2004, 24(4): 480.]
- [71] Gao F Y, Jia J, Xia D S, et al. Asynchronous Holocene climate optimum across mid-latitude Asia[J]. Palaeogeography, Palaeoclimatology, Palaeoecology, 2019, 518: 206-214.
- [72] Liang P, Yang X P. Landscape spatial patterns in the Maowusu (Mu Us) sandy land, northern China and their impact factors [J]. Catena, 2016, 145: 321-333.
- [73] Wang H P, Chen J H, Zhang X J, et al. Palaeosol development in the Chinese Loess Plateau as an indicator of the strength of the East Asian summer monsoon: Evidence for a mid-Holocene maximum[J]. Quaternary International, 2014, 334-335: 155-164.
- [74] Yang L H, Wang T, Zhou J, et al. OSL chronology and possible forcing mechanisms of dune evolution in the Horqin dune-field in northern China since the Last Glacial Maximum[J]. Quaternary Research, 2012, 78(2): 185-196.
- [75] Guo L C, Xiong S F, Ding Z L, et al. Role of the mid-Holocene environmental transition in the decline of Late Neolithic cultures in the deserts of NE China[J]. Quaternary Science Reviews, 2018, 190: 98-113.
- [76] 王苏民, 吴瑞金, 蒋新禾. 内蒙古岱海末次冰期以来的环境变迁与古气候[J]. 第四纪研究, 1990, 10(3): 223-232. [Wang Sumin, Wu Ruijin, Jiang Xinhe. Environment evolution and paleoclimate of Daihai lake, Inner Mongolia since the Last Glaciation[J]. Quaternary Sciences, 1990, 10(3): 223-232.]
- [77] 李华章, 刘清泗, 汪家兴. 内蒙古高原黄旗海、岱海全新世湖泊演变研究[J]. 湖泊科学, 1992, 4(1): 31-39. [Li Hua-zhang, Liu Qingsi, Wang Jiaxing. Study of evolution of Huangqihai and Daihai lakes in Holocene in Inner Mongolia Plateau[J]. Journal of Lake Sciences, 1992, 4(1): 31-39.]
- [78] Wu H N, Ma Y Z, Feng Z D, et al. A high resolution record of vegetation and environmental variation through the last~25,000 years in the western part of the Chinese Loess Plateau [J]. Palaeogeography, Palaeoclimatology, Palaeoecology, 2009, 273(1/2): 191-199.
- [79] Wu W X, Liu D S. 5500 A BP climatic event and its implications for the emergence of civilizations in Egypt and Mesopotamia and Neolithic cultural development in China[J]. Earth Science Frontiers, 2002, 9(1): 155-162.
- [80] 曹建廷, 沈吉, 王苏民. 内蒙古岱海气候环境演变的沉积记录[J]. 地理学与国土研究, 1999, 15(3): 82-86. [Cao Jian-yan, Shen Ji, Wang Sumin. Sedimentary records of climate and environmental evolution in Daihai, Inner Mongolia[J]. Geography and Territorial Research, 1999, 15(3): 82-86.]
- [81] Broecker W S. Was the medieval warm Period global?[J]. Science, 2001, 291(5508): 1497-1499.

Optically Stimulated Luminescence Chronology and Climate Change in the Otindag Sandy Land Since the Last Glacial Maximum

TIAN YaQi¹, ZHOU YaLi¹, SUN XiaoWei¹, ZHANG YueMin¹, CHUI YuDa²

1. School of Geography and Tourism, Shaanxi Normal University, Xi'an 710119, China

2. Institute of Earth Environment, Chinese Academy of Sciences, Xi'an 710061, China

Abstract: [Objective] The Otindag sandy land, located at the boundary of the East Asian monsoon region in east-central Inner Mongolia, is an ideal area for studying climate change since the Last Glacial Maximum owing to its unique geographical environment and extensive development of aeolian sand stratigraphy. Previous studies on the chronology of the Otindag sandy land have focused on the Holocene, and relatively few studies have been conducted since the Last Glacial Maximum owing to the lack of a systematic stratigraphic chronology framework, and the scientific issue of whether the Holocene Climate Optimum in the sandy land began in the Early or Middle Holocene. This remains controversial, based on different dating methods and research objects. [Methods] In this study, two aeolian sand sedimentary sequences on the southern edge of the Otindag sandy land, Lanqi South (LQS) and Baleng Mountain (BLS), were studied, and the stratigraphic chronological framework was determined by the single-aliquot regenerative-dose (SAR) method with the optical stimulated luminescence (OSL) dating method. Combined with the sedimentary characteristics, grain size and quartz grain surface morphological features were integrated for analysis. [Results] The results show that: from 18 to 11.5 ka, solar radiation and East Asian summer monsoon gradually increased, aeolian sand and sandy loess interstratification were developed, with a cold and dry climate, strong sand-storm activity, and millennial-scale climate fluctuations. The aeolian sand and sand loess, which developed at 15.9 and 12.2 ka, correspond well to two significant cooling and dehumidification events during the temperature warming of the last deglaciation period. Between 11.5 ka and 8.2 ka, the temperature fluctuated and increased, with a relatively dry and cold climate and primarily developed aeolian sands with sandy paleosols. The sandy paleosoil developed at 8.2 ka and 8.94 ka indicated the early Holocene, and the sandy climate gradually changed from cold and dry to warm and wet. The lacustrine and aeolian sand developed at approximately 10 ka are contemporaneous heterogeneous sediments, both indicating a cold and dry climate, and their formation was influenced by three depositional dynamics: wind, river and lake. From 8.2 to 2.7 ka, solar radiation reached its maximum, the East Asian summer monsoon strengthened, and the climate was the warmest and wetter. The sandy paleosols were developed in both profiles. Since 2.7 ka, the solar radiation has weakened, the East Asian winter monsoon has strengthened, the climate has become mild and dry, and weak sandy paleosols have developed. The sandy paleosols developed at approximately 1 ka are consistent with the medieval warm period. The formation of lacustrine sediments in LQS profile was mainly influenced by local geomorphology, which is similar to the coexistence of dunes and lakes in modern sandy land. [Conclusions] In general, the Holocene Climate Optimum in Otindag sandy land was in the middle of Holocene. The rapid climate change since the Last Glacial Maximum in the Otindag sandy land has global and universal characteristics, which are a regional response to global climate change and closely related to the East Asian monsoon, driven by solar radiation and global ice volume.

Key words: Otindag sandy land; optical simulated luminescence (OSL) dating; Last Glacial Maximum; climate change